THE JOURNAL OF PHYSICAL CHEMISTRY A
A JOURNAL OF THE AMERICAN CHEMICAL SOCIETY

pubs.acs.org/JPCA

Article

An Infrared Study of Gas-Phase Metal Nitrosyl Ion−Molecule Complexes

Published as part of The Journal of Physical Chemistry virtual special issue "Marsha I. Lester Festschrift".

Gabriele Meizyte, Philip A. J. Pearcy, Peter D. Watson, Edward I. Brewer, Alice E. Green, Matthew Doll, Olga A. Duda, and Stuart R. Mackenzie*

Cite This: *J. Phys. Chem. A* 2022, 126, 9414−9422

Read Online

ACCESS | Metrics & More | Article Recommendations | Supporting Information

ABSTRACT: We present a combined experimental and quantum chemical study of gas-phase group 9 metal nitrosyl complexes, $M(NO)_n^+$ (M = Co, Rh, Ir). Experimental infrared photodissociation spectra of mass-selected ion-molecule complexes are presented in the region 1600 cm^{-1} to 2000 cm^{-1} which includes the NO stretch. These are interpreted by comparison with the simulated spectra of energetically low-lying structures calculated using density functional theory. A mix of linear and nonlinear ligand binding is observed, often within the same complex, and clear evidence of coordination shell closing is observed at n = 4 for $Co(NO)_n^+$ and $Ir(NO)_n^+$. Calculations of $Rh(NO)_n^+$ complexes suggest additional low-lying five-coordinate structures. In all cases, once a second coordination shell is occupied, new spectral features appear which are assigned to $(NO)_2$ dimer moieties. Further evidence of such motifs comes from differences in the spectra recorded in the dissociation channels corresponding to single and double ligand loss.

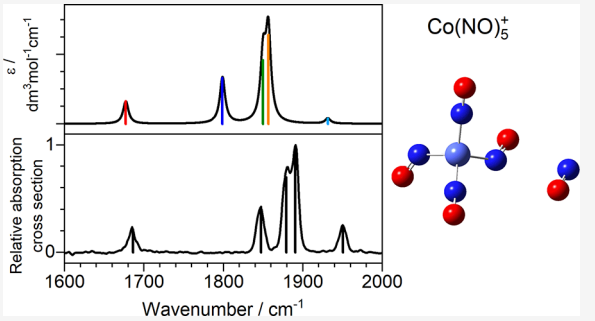

1. INTRODUCTION

Nitrogen oxides (NO_x) are well-known for their detrimental effects on the environment and as a major source of air pollution harmful to human health.[1,2] Although formed naturally, e.g., in lightning and/or forest fires, anthropogenic sources represent a significant fraction of NO_x production. Both NO_2 and NO are generated by the internal combustion engine, and this has led to the introduction of stringent emission controls.[3,4] Current mitigation strategies include the widespread use of automobile catalytic converters which harness surface catalytic chemistry of finely dispersed transition metals.[5,6] In turn, this has stimulated extensive research aimed at developing a better understanding of this chemistry including that of nitric oxide, NO, the subject of this work. For its role in both the environment and in biology, NO was named *Science* magazine's molecule of year for 1992[7] and a whole edition of *Chemical Reviews* was dedicated to NO chemistry.[8]

Atomic ions and small gas-phase metal clusters can represent tractable model systems, providing molecular level insight into fundamental metal−ligand interactions, including those important in catalytic chemistry, free of complications arising from substrates, solvation, or aggregation.[9] The thermal reactivity of NO with a wide range of gas-phase metal cations has been studied by Bohme and co-workers by inductively coupled plasma/selected-ion flow tube (ICP/SIFT) tandem mass spectrometry.[10] This revealed extensive and varied chemistry involving electron donation and both atom acceptor and donor reactions. Relevant to the metal centers studied here, a mix of molecular and dissociative NO binding on Co_n^+ clusters has been observed under different conditions.[11−14] $Rh_n^±$ reactions with NO have been studied extensively under single[15−17] and multiple collision conditions, and the chemistry has been reviewed recently.[18] There have also been spectroscopic studies of NO binding to Au_n^+ and Ir_n^+ clusters.[19,20]

NO is an intriguing ligand in coordination chemistry. A kinetically inert, stable radical, it exhibits a range of different binding motifs, coordinating formally via one- or three-electron donation, and nitrosyl complexes often exhibit very different chemistry to their carbonyl analogues.[21] The open-shell nature of nitric oxide presents particular challenges for quantum chemical calculations. Blanchet et al. employed density functional theory (DFT) to study first row transition metal atom-NO molecules. They established nonlinear binding

Received: October 14, 2022
Revised: November 21, 2022
Published: December 8, 2022

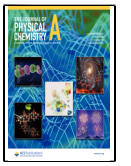

through the N atom in CoNO arising from the Co 3d and 4s orbitals with the highest occupied 5σ orbital in NO with a triplet ground state favored due to symmetry breaking.[22] Bauschlicher and Hall applied DFT and coupled cluster calculations to the equivalent cationic species and, for $CoNO^+$, found a linear geometry preferred.[23]

This work presents an infrared photodissociation (IR-PD) study of NO binding to group 9 cations $Co(NO)_n^+$, $Rh(NO)_n^+$, and $Ir(NO)_n^+$ (n = 3−7) with interpretation aided by comparison with simulated spectra of low-energy structures calculated by DFT. The present work follows detailed IR-PD studies of $M(NO)_n^+$ (M = Fe, Cu, Ag, and Au) complexes by Zhou and co-workers which showed marked differences in the structures adopted for different metal ions.[24−26] $Fe(NO)_n^+$ structures exhibit linear (three-electron) binding until closure of the first coordination shell is achieved at 4, with the messenger Ar tag atoms leading to strong distortions.[24] $Cu(NO)_n^+$ complexes are characterized by bent (one-electron) binding and significant ligand−ligand interactions with clear evidence of bidentate dimer $(NO)_2$ ligand.[25] Nonlinear ligand binding and dimer structures were also observed in $Ag(NO)_n^+$ and $Au(NO)_n^+$ complexes albeit with first coordination shells of 4 and 2, respectively.[26]

2. EXPERIMENTAL AND COMPUTATIONAL METHODS

The experimental setup has been described in detail previously[27,28] and modified recently to include the mass selection of ions via a quadrupole mass filter.[29] Briefly, a rotating disc target of the required metal (Co, Rh, or Ir) is ablated at 532 nm by a pulsed Nd:YAG laser (10 Hz, ca. 2−10 mJ as necessary). Ablated species are entrained in a gas pulse of Ar seeded with 1−5% NO which expands into the vacuum forming a molecular beam with the higher NO mole fractions required for efficient generation of $Ir(NO)_n^+$. The beam is skimmed before passing through a quadrupole mass filter−quadrupole bender assembly and then entering the extraction region of a reflectron time-of-flight (ToF) mass spectrometer.

To record IR-PD spectra, the cluster beam is subjected to tunable pulsed infrared radiation from a tabletop optical parametric oscillator/optical parametric amplifier (OPO/OPA, Laservision) system, operating in the 1600−2000 cm^{-1} range. Following mass-selection of the parent ion−molecule complex, spectra are recorded as a function of wavenumber in the daughter fragment channels against a zero background.

To account for variations in the infrared pulse energy across the wavenumber region scanned, spectra are reported here in terms of a normalized cross-section in a given fragment channel using a modified Beer−Lambert law:[30]

$$\sigma = -\frac{\log\left(1 - \frac{N_f}{\alpha N_0}\right)}{\Phi} \quad (1)$$

in which σ is the absorption cross-section, N_f and N_0 correspond to the intensity of the fragment and parent signals, respectively, and Φ is the photon flux. The factor α describes the overlap between the ion beam, and the infrared beam and is assumed to be 1. Spectra are normalized to the strongest peak in the spectrum.

To aid assignment, experimental $M(NO)_n^+$ IR-PD spectra are compared with simulated spectra of energetically low-lying structures determined from DFT using the Gaussian 16 software package[31] with novel potential structures generated by a modified KICK algorithm.[32] It is worth noting that open-shell ligands such as NO pose particular difficulties for DFT, as complexes often give rise to multiple low-lying electronic states as well as large numbers of isomeric forms.[33] The B3P86[34,35]/def2TZVP[36,37] functional/basis set combination was used throughout, having proven reliable in similar studies by our group.[38,39] To provide a better match with experimental data, computed harmonic vibrational frequencies were scaled by a factor of 0.9347, determined by calculating the vibrational frequency of the free NO stretch which is found experimentally at 1876 cm^{-1}.[40] Calculated spectral lines are convoluted with Lorentzian line shapes with full width half-maximum (fwhm) = 8 cm^{-1} to aid comparison with spectra. All energies reported here include zero-point energy corrections. Only molecularly bound ligands have been considered, as these are the only structures expected to exhibit spectra in our experimental region. Dissociatively bound complexes lie substantially lower in energy, but access to these minima is kinetically hindered by large activation barriers.

3. RESULTS AND DISCUSSION

A. Time-of-Flight Mass Spectra. A typical time-of-flight mass spectrum produced by laser ablation of a Co target in the presence of NO seeded in Ar is given in Figure 1. The mass spectrum is dominated by the $Co(NO)_n^+$ peaks. Smaller mass species are favored under expansion conditions used here, with a marked drop in signal intensity for n > 4 which is suggestive of a first coordination sphere of four ligands. Consistent with the reactivity study of Bohme and co-workers, CoO^+ and $CoONO^+$ are also formed in significant number densities[10] along with several Ar-tagged species.

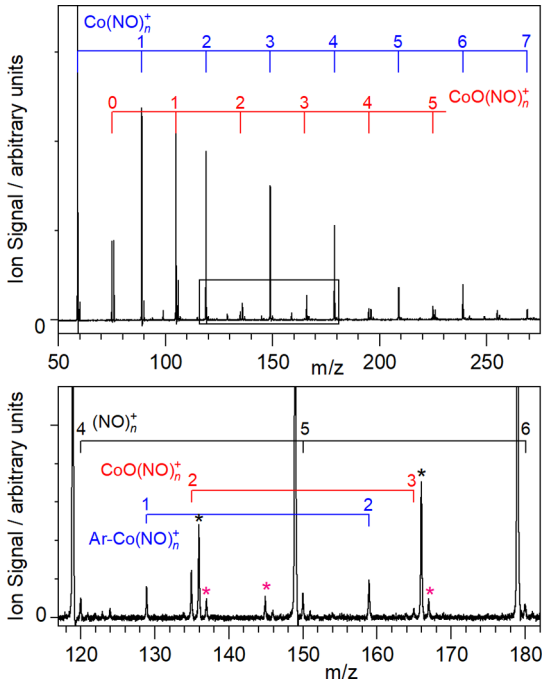

Figure 1. Time-of-flight mass spectrum produced upon ablating the Co metal target in the presence of NO in Ar gas mix (1.5%). The lower panel shows an expanded region indicated in the top panel. Other species observed include $[O(NO)_n]^+$ complexes (black asterisks), Ar-tagged peaks and water-containing species (red asterisks).

https://doi.org/10.1021/acs.jpca.2c07228
J. Phys. Chem. A 2022, 126, 9414−9422

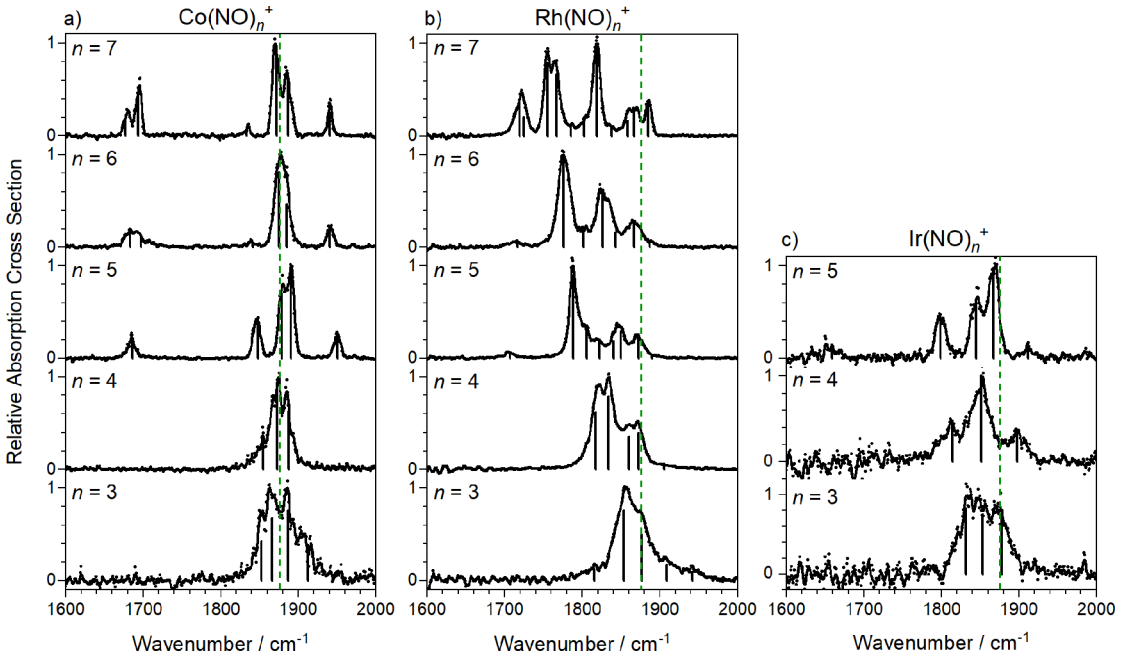

Figure 2. Infrared photodissociation spectra of (a) Co(NO)$_n^+$, (b) Rh(NO)$_n^+$, and (c) Ir(NO)$_n^+$ complexes, recorded in the enhancement of the M(NO)$_{n-1}^+$ daughter channel and shown as normalized relative absorption cross-sections for each complex size. Vertical lines arise from fitting of the spectrum to Gaussian functions. Green dashed lines indicate the wavenumber of the free NO stretch at 1876 cm^{-1}.[41]

Mass spectra obtained following Rh and Ir ablation can be found in Supporting Information. The rhodium mass spectrum is cleaner than that for cobalt and is dominated by the progression of Rh(NO)$_n^+$ (n = 0−7) peaks whose intensity decrease monotonically with n with little obvious sign of clear coordination shells. Of the oxides, only [RhO(NO)$^+$] is formed in significant number density. Iridium has two stable isotopes of 191 u and 193 u, and this complicates the mass spectrum. Even so, the mass spectrum is markedly richer than the cobalt and rhodium. Below m/z = 300 the mass spectrum is dominated by strong Ir(NO)$_n^+$ and IrO(NO)$_n^+$ signals, the latter reflecting the O atom transfer reactivity of Ir$^+$ toward nitric oxide.[10] Perhaps as a result of this reactivity it proved impossible to generate Ir(NO)$_n^+$ (n > 5) in sufficient number density to record infrared spectra with acceptable signal-to-noise ratio.

In all mass spectra there is evidence for naked (NO)$_n^+$ and NO$_2$(NO)$_n^+$ clusters. These are produced within the ablation plasma, and their infrared action spectra will be the subject of a future study.

B. Infrared Spectra of M(NO)$_n^+$ Ion−Molecule Complexes. An overview of the infrared action spectra of M(NO)$_n^+$ (M = Co, Rh, Ir) complexes is shown in Figure 2. In all cases the dominant fragmentation observed following photoexcitation is NO loss, and the spectra shown are recorded against a zero background in enhancement in the daughter M(NO)$^+_{n-1}$ (i.e., simple NO loss) mass channel. Vertical lines shown under each spectrum represent the centers of Gaussian functions used to fit to the spectra from which trends in band positions can be extracted as well as providing an estimate of the number of bands contributing. For each spectrum, the full width at half-maximum was fixed to that of the most highly resolved band and the number of bands was guided by the number of infrared active modes in simulated spectra.

Negligible fragmentation was observed for the very smallest, n = 1, 2 complexes. This is common in IR-PD and reflects the fact that the first few ligands typically bind strongly to a metal center and that many photons are required to dissociate the complex. In the present case, the binding energies of each of the first two nitrosyl ligands is ≥1.4 eV (see Supporting Information), while the photon energy in this spectral region is ca. 0.20−0.25 eV (of course, the complexes have significant internal energy of their own). For similar reasons, the spectra of the n = 3, 4 complexes exhibit comparatively poor signal-to-noise ratios, reflecting their own weak fragmentation efficiency. Their broad, partially resolved appearance suggests that in these cases, too, multiple photons are needed to drive NO loss. By contrast, the infrared spectra of the larger M(NO)$_n^+$ (M= Co, Rh, Ir, n ≥ 5) complexes are both significantly better resolved and exhibit higher signal-to-noise ratios. This is consistent with the binding energy of the fifth (and higher) NO ligand being comparable with the IR photon energy (see Supporting Information).

The evolution of the Co(NO)$_n^+$ and Ir(NO)$_n^+$ spectra with cluster size is similar with most intensity observed close to the free NO stretch at 1876 cm^{-1} and new features appearing for larger complexes. In these regards the spectra are very similar to those reported previously for Fe(NO)$_n^+$.[24] The Rh(NO)$_n^+$ spectra, by contrast, are qualitatively different, and although there is a persistent band around the free NO stretch, a noticeable overall red shift in the IR spectrum is observed with increasing n and any satellite bands are much less prominent.

In the spectra of Co(NO)$_n^+$ complexes, a new pair of bands appears for larger (n ≥ 5) complexes with one band around 1680 cm^{-1} and another near 1950 cm^{-1}. Similar pairs of bands are visible in the Ir(NO)$_5^+$ spectrum and, to a lesser extent, the Rh(NO)$_n^+$ (n > 4) spectra. Zhou and co-workers have also reported very similar bands in the spectra of M(NO)$_n^+$ (M = Au, Ag, Cu, Fe). These bands have been attributed to the formation of a dimer, (NO)$_2$, motif forming following closure

https://doi.org/10.1021/acs.jpca.2c07228
J. Phys. Chem. A 2022, 126, 9414−9422

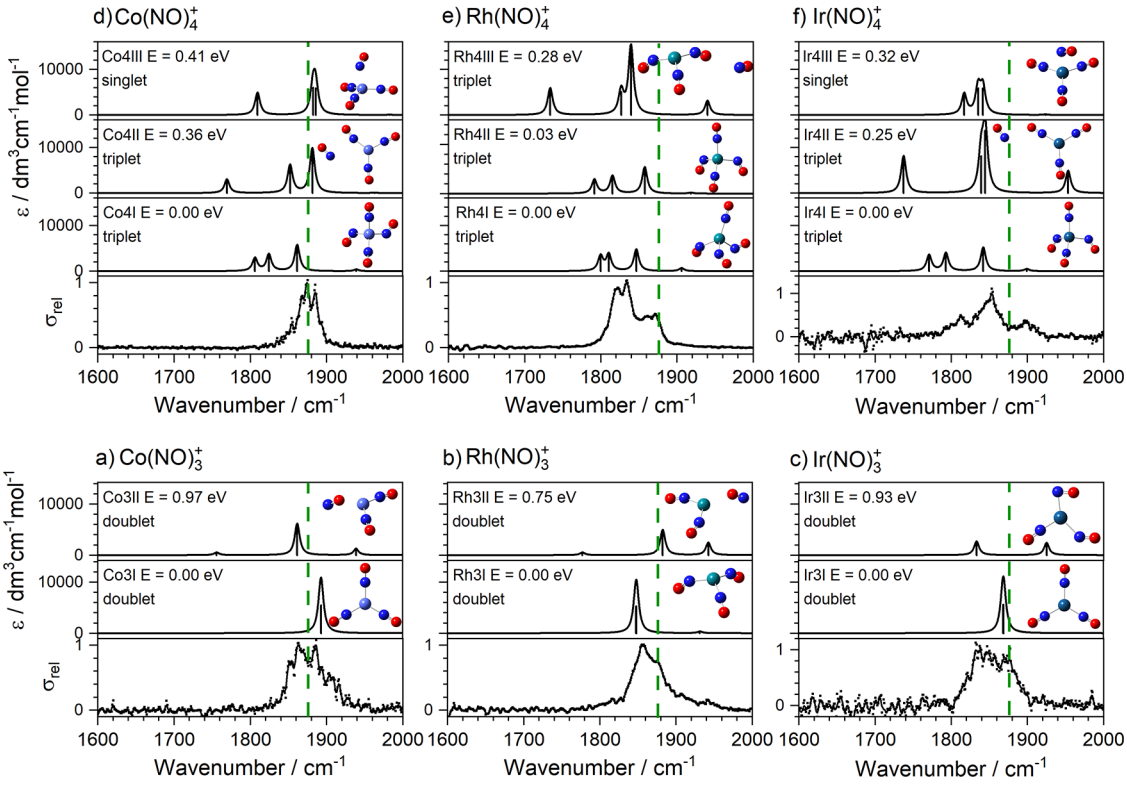

Figure 3. Comparison of experimental and simulated spectra for $M(NO)_n^+$ (M = Co, Rh, Ir; n = 3 (a–c), 4 (d–f)) complexes showing the lowest energy calculated structures only. Green dashed lines indicate the wavenumber of the free NO stretch at 1876 cm^{-1}.[40]

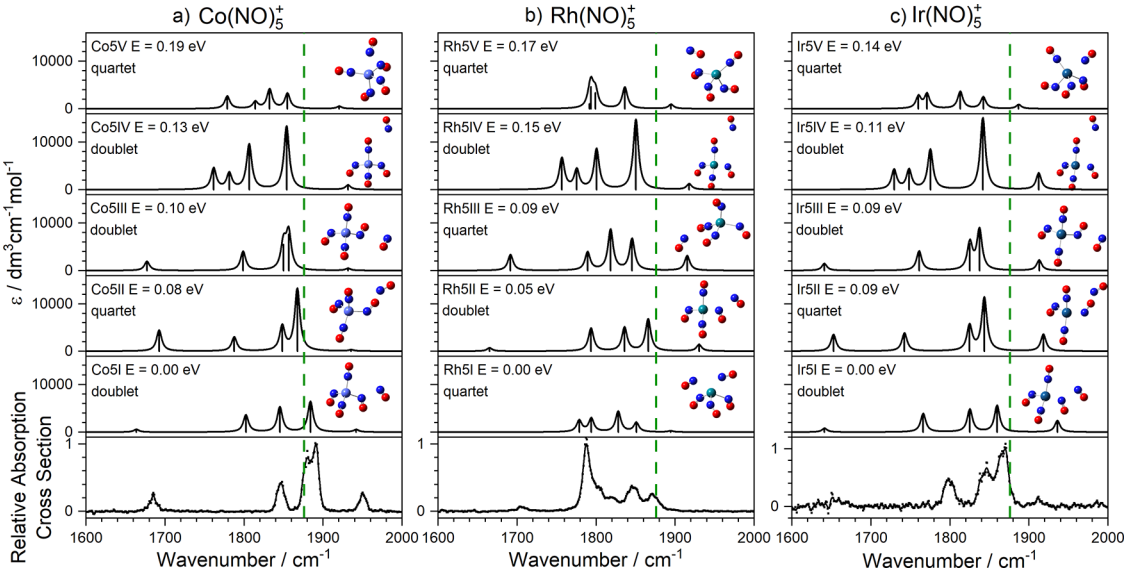

Figure 4. Comparison of experimental and simulated spectra of low-lying isomers for (a) $Co(NO)_5^+$, (b) $Rh(NO)_5^+$, and (c) $Ir(NO)_5^+$. In most cases the fifth ligand binds more weakly in a second coordination shell giving rise to new spectral features. Green dashed lines indicate the wavenumber of the free NO stretch at 1876 cm^{-1}.[40]

of the inner coordination shell.[24−26] The appearance of these bands is thus consistent with an inner coordination shell of four with the fifth ligand forced to start a new coordination shell and binding preferentially to one of the inner-shell ligands.

C. Comparison of Experimental and Simulated Spectra. The binding of the NO radical at charged metal centers is a complex balance of many contributing factors. The dominant electrostatic interaction is the charge−dipole attraction which favors N-binding with the proximity of the metal cation strongly polarizing the NO bond. In addition, there are multiple components of incipient chemical bonding arising from (i) NO lone-pair σ donation, (ii) π donation from the unpaired NO π^* electron, and (iii) π-back bonding from the occupied d orbitals on the metal center into the NO π^* orbitals. The relative contributions of these factors lead to subtle structural differences which are reflected in the infrared spectra. For example, σ-donation, in which NO acts formally as

https://doi.org/10.1021/acs.jpca.2c07228
J. Phys. Chem. A 2022, 126, 9414−9422

a three-electron donor, leads to near linear M^+−N═O binding. By contrast, one-electron π^*-donation leads to nonlinear coordination.[42] The latter was found to dominate the structures of the coinage-metal nitrosyl complexes[25,26] while a mix of the two was invoked to interpret the spectra of $Fe(NO)_n^+$.[24]

Figure 3 shows a comparison of experimental and simulated spectra for the $M(NO)_n^+$ (M = Co, Rh, Ir, n = 3, 4) complexes. Extended versions of this figure with additional (higher-lying) calculated structures and electronic states are provided in Supporting Information. Notwithstanding the broad, unresolved nature of the experimental spectra, a few clear conclusions can be drawn. For n = 3 complexes, all low energy structures (within the lowest 1 eV) have doublet multiplicity. A clear lowest energy isomer is identified, labeled M3I (M = Co, Rh, Ir), whose simulated spectrum accounts well for that observed. Co3I and Ir3I are planar D_{3h} structures with rigidly linear ligand binding indicating the dominance of (three-electron) σ-donation. By contrast, the bent C_{3v} Rh3I reflects π-donation. There is negligible evidence of ligand activation in either the wavenumber of the spectral bands or the calculated NO bond lengths. In all cases ligands bind via the nitrogen atom with, at most, weak evidence for the presence of energetically higher-lying O-bound structures.

The lowest energy $M(NO)_4^+$ structures are all triplet multiplicity, tetrahedral-based, N-bound structures. We calculate low-lying excited electronic states for each species (see Supporting Information) as well as multiple isomeric structures on the ground-state surface, some of which include a second coordination shell (e.g., Co4II, Rh4III, and Ir4II). There is, however, little evidence for these structures in the experimental spectra. In both $Co(NO)_4^+$ and $Ir(NO)_4^+$ the lowest energy structures identified (Co4I and Ir4I) have two linear and two nonlinear bound ligands. Again, though, the effect on the bond lengths is negligible. The equivalent $Rh(NO)_4^+$ structure (Rh4II) lies just 0.03 eV higher than the lowest energy Rh4I structure, with three of its ligands bound nonlinearly. There is little in the experimental spectrum to distinguish between them, and it is possible that both are present.

With the addition of a fifth ligand, our calculations show the opening of a second coordination shell and binding in dimer motif to one of the inner ligands (Figure 4). The exception is the lowest energy calculated structure for $Rh(NO)_5^+$ (structure Rh5I) which shows a five-coordinate structure. The weaker binding in the second shell gives rise to a richer distribution of both low-lying electronic states (doublet and quartet states) and structural isomers predicted as shown in Figure 4. In all cases, the signature of the $(NO)_2$ motif is provided by the new vibrational bands, most prominent in the spectrum of $Co(NO)_5^+$ at 1680 and 1950 cm^{-1} but also visible in the other two complexes.

In the case of $Co(NO)_5^+$ and $Ir(NO)_5^+$ there is convincing agreement between the experimental spectrum and that of the energetically low-lying structures. Figure 5 shows one such comparison for the $Co(NO)_5^+$ spectrum with the simulated spectrum of structure Co5III (E = 0.1 eV above the lowest energy calculated structure). This structure exhibits an NO-dimer in trans form though the isomerism of the dimer has very minor effect on the spectrum. Figure 5 also depicts the ligand vibrations responsible for the five high frequency infrared active bands in this region (labeled A−E). The A mode at ca. 1680 cm^{-1} is highly localized and arises from the antisymmetric motion of the two ligands comprising the dimer

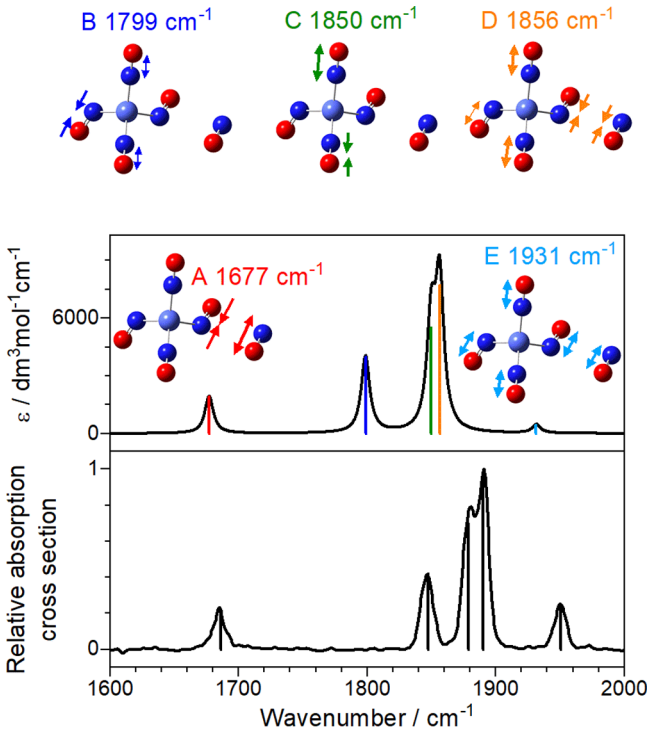

Figure 5. A comparison of the experimental and computational spectrum (Co5III) for $Co(NO)_5^+$ with color-coded mode vectors.

moiety. The red-shift in this band reflects weak activation of the inner of the two dimer ligands whose bond length (1.146 Å) is slightly longer than that of its partner (1.119 Å). The B mode comprises out-of-phase vibrations of the three nondimer ligands, mainly that opposite the dimer. The C mode (calculated at 1850 cm^{-1}, observed at 1880 cm^{-1}) involves out-of-phase motion of the two near linear bound ligands. Finally, the two highest frequency modes, D and E, comprise concerted motion of all ligands with the symmetric vibration in the dimer either in-phase (mode E) or out-of-phase (D) with the other ligands. A mode analogous to the symmetric "breathing" mode E appears in the simulated spectra of all tetrahedral n = 4 complexes, but in this case it gains oscillator strength from the lower symmetry arising from the fifth ligand.

The lowest energy calculated structures (and, thus, spectra) of $Ir(NO)_n^+$ are very similar to those of the $Co(NO)_n^+$ complexes (Figure 4). The agreement between simulated and experimental spectra is not quite as good for the $Rh(NO)_n^+$ complexes, but the dimer motif is almost certainly signified by the band around 1700 cm^{-1}. No single isomer provides as convincing a fit as that for the $Co(NO)_5^+$ complex in Figure 5. In particular, the most intense feature at 1790 cm^{-1} is missing from most simulated spectra. However, even a small frequency shift in a single band (for example, in the spectra of structures Rh5I or Rh5 V) would recover it.

The spectra of the $Co(NO)_n^+$ complexes do not change markedly as sixth and seventh ligands bind, with the exception of the dimer band around 1680 cm^{-1} which splits into (at least) two bands as more dimer moieties form. Figures 6 and 7 contain the comparison of experimental and simulated spectra for energetically low-lying structures of n = 6, 7 complexes, respectively. The spectra of the $Rh(NO)_n^+$ complexes continue more significant evolution with additional ligands. The trend for the overall spectrum to shift further red of the free NO

https://doi.org/10.1021/acs.jpca.2c07228
J. Phys. Chem. A 2022, 126, 9414−9422

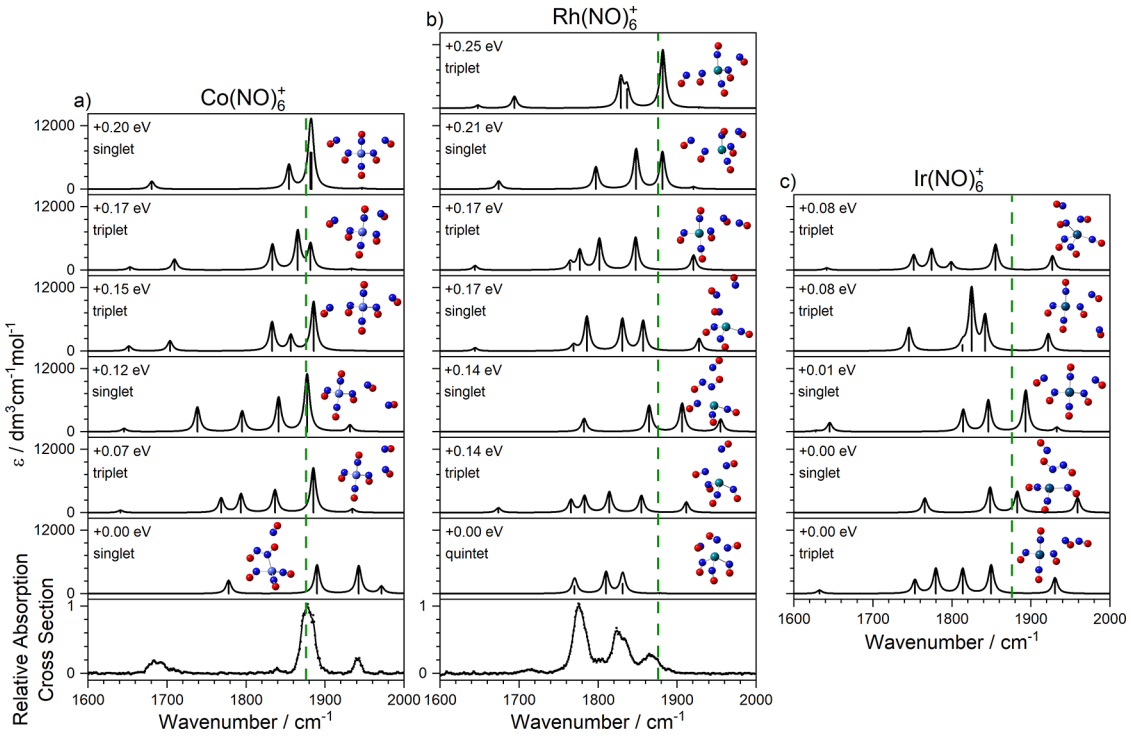

Figure 6. Comparison of experimental and simulated spectra of low-lying isomers for (a) $Co(NO)_6^+$, (b) $Rh(NO)_6^+$, and (c) $Ir(NO)_6^+$. Green dashed lines indicate the wavenumber of the free NO stretch at 1876 cm^{-1}.[40]

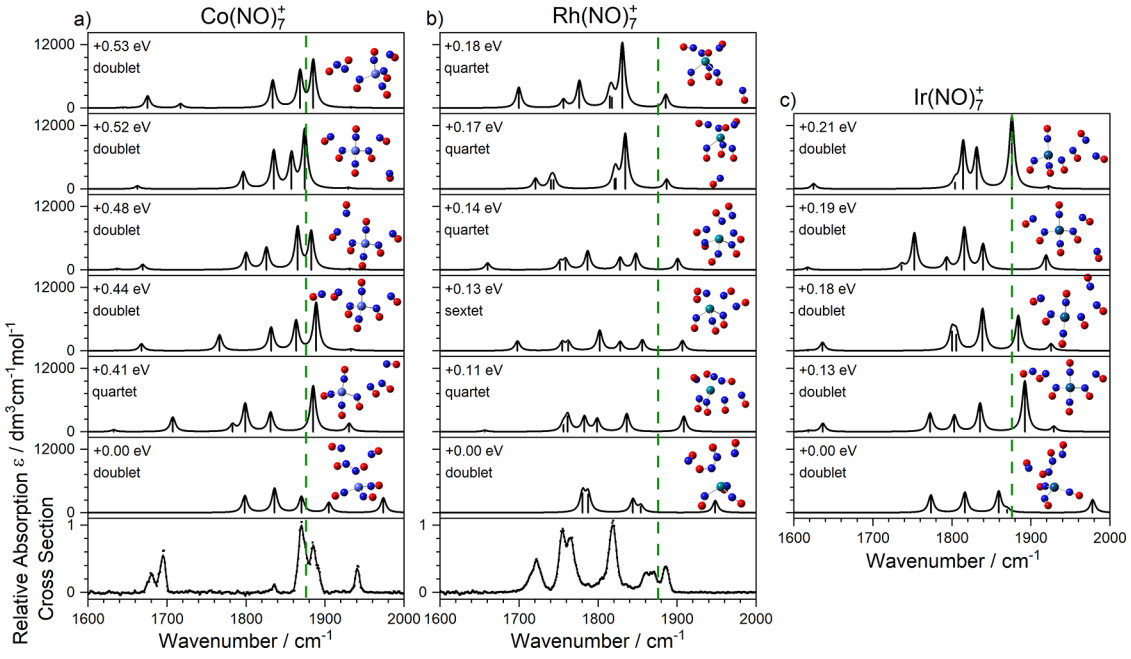

Figure 7. Comparison of experimental and simulated spectra of low-lying isomers for (a) $Co(NO)_7^+$, (b) $Rh(NO)_7^+$, and (c) $Ir(NO)_7^+$. Green dashed lines indicate the wavenumber of the free NO stretch at 1876 cm^{-1}.[40]

stretch continues, and more low-lying electronic states are predicted than for Co^+ or Ir^+ complexes. The origin of the increased red-shift observed in the spectra of $Rh(NO)_n^+$ complexes may lie in the increased propensity for nonlinear (one-electron) binding with Rh^+. As a result, the addition of more ligands leads to more effective back-bonding into the NO π^* system. This is consistent with the smaller spectral shifts and reduced intensity of the dimer bands in the $Rh(NO)_n^+$ complexes. Despite the apparent simplicity of the spectra observed, however, it is difficult to make unambiguous assignments beyond the presence of dimer structures, and it seems likely that more than one isomer and/or electronic state is present.

D. Different Dissociation Channels. The spectra shown above in Figures 2−7 were all recorded in the daughter fragment channel corresponding to the loss of a single NO ligand. In some cases, especially for larger complexes, weaker additional fragment channels were observed which provide

https://doi.org/10.1021/acs.jpca.2c07228
J. Phys. Chem. A 2022, 126, 9414−9422

additional information on the structure of the complex. At a basic level, the degree of fragmentation observed provides additional information on coordination shells with the $Co(NO)_n^+$ ($n > 6$) showing loss of two ligands consistent with a first coordination shell of 4 (see Supporting Information).

Further structural information is provided by the spectra recorded in the −2(NO) (*i.e.*, double ligand loss) fragmentation channels for $Co(NO)_n^+$ ($n = 6, 7$) and $Rh(NO)_n^+$ ($n = 6, 7$) as shown in Figure 8. In the $Co(NO)_n^+$ spectra at least

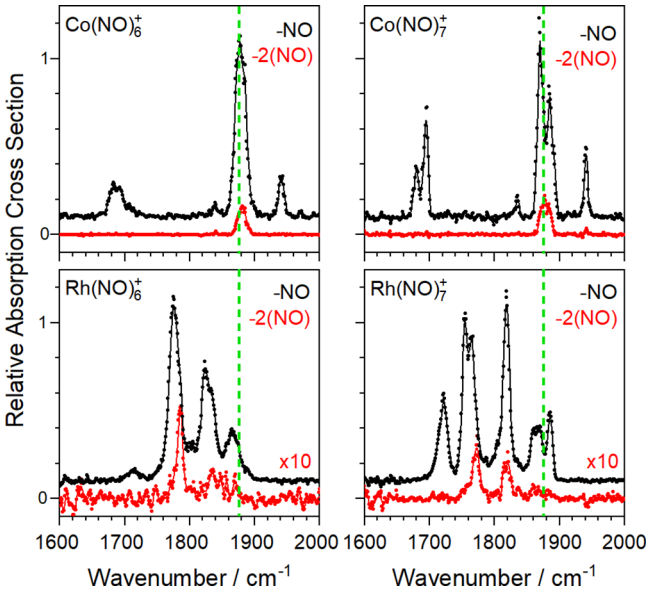

Figure 8. IR-PD spectra of $Co(NO)_n^+$ ($n = 6–7$) (upper panels) and $Rh(NO)_n^+$ ($n = 6–7$) (lower panels) species, recorded in different fragmentation channels: −NO (black line), −2(NO) (red line). Spectra are given in terms of normalized absorption cross-sections for the −NO channel (black line), and the other channel is scaled accordingly as shown. The NO loss channel spectrum data is shown offset vertically for clarity. Green dashed lines indicate the wavenumber of the free NO stretch at 1876 cm^{-1}.[40]

some components of the strong bands in the central (1750–1900 cm^{-1}) spectral region appear in both the single, −(NO), and the double, −2(NO), loss channel. The same is true in the $Rh(NO)_n^+$ spectra though some of the bands are noticeably narrower and slightly blue-shifted in the −2(NO) channel. It is possible that only one spectral component in a blended band is observed in the double-loss channel. In all cases, however, the peripheral bands, while clear in the −NO loss channel, are essentially absent in the −2(NO) spectra. We interpret this as further confirmation that the outer spectral bands in the spectrum (especially the low frequency band) arise from the dimer moiety (see Figure 5). In these bands, once a first photon is absorbed, a ligand from the outer coordination shell is lost and, with it, crucially the chromophore itself. As a result, no subsequent photon can be absorbed at the same wavenumber to remove a second ligand. These results strongly suggest that the dimer $(NO)_2$ moiety itself is not lost as an intact entity but rather the −2(NO) channel comprises two sequential single loss processes. This is consistent with the strength of binding direct to the metal center exceeding the one-photon energy. By contrast, the more central IR modes, which do not involve motion of the dimer (See Figure 5), can absorb more than one photon, leading to the loss of two ligands. In this way, differences in the spectra recorded in different fragment mass channels provide exquisite detail on the nature of the vibrational mode excited.

4. CONCLUSIONS

A comparison of infrared action spectra with simulated spectra of calculated low energy isomers has revealed the structures of $M(NO)_n^+$ (M = Co, Rh, Ir) ion−molecule complexes. Notwithstanding the difficulties of applying DFT to multiple open-shell ligands, some clear structural features are observed, including evidence of complete coordination shells. A mix of linear and nonlinear ligand binding motifs is also observed, often within the same complex, and a range of energetically low-lying isomers and/or electronic states is found for all complexes with $n \geq 4$. The $Co(NO)_n^+$ and $Ir(NO)_n^+$ complexes exhibit similar spectra/structures throughout the size range studied. The spectra of the $Rh(NO)_n^+$ complexes appear qualitatively different which may result from an increased propensity for nonlinear (one-electron) ligand binding.

In common with previous studies of gas-phase metal nitrosyl complexes, there is clear evidence for the formation of NO dimers once binding in a second coordination shell occurs at $n \geq 5$. New spectral features appear that are not present in the spectra of smaller complexes, including a strongly red-shifted band (≤1700 cm^{-1}). Further evidence for some of the vibrational mode assignments comes from the difference in the action spectra observed in different fragmentation channels, illustrating the benefits of parent ion mass-selection.

■ ASSOCIATED CONTENT

Supporting Information

The Supporting Information is available free of charge at https://pubs.acs.org/doi/10.1021/acs.jpca.2c07228.

Additional time-of-flight spectra, computational structure details, comparison of experimental and simulated spectra for additional complex sizes, photofragment time-of-flight spectra, relative energy of electronic states (PDF)

■ AUTHOR INFORMATION

Corresponding Author

Stuart R. Mackenzie − *Department of Chemistry, University of Oxford, Physical and Theoretical Chemistry Laboratory, Oxford, United Kingdom OX1 3QZ;* orcid.org/0000-0002-3166-8631; Email: stuart.mackenzie@chem.ox.ac.uk

Authors

Gabriele Meizyte − *Department of Chemistry, University of Oxford, Physical and Theoretical Chemistry Laboratory, Oxford, United Kingdom OX1 3QZ*

Philip A. J. Pearcy − *Department of Chemistry, University of Oxford, Physical and Theoretical Chemistry Laboratory, Oxford, United Kingdom OX1 3QZ*

Peter D. Watson − *Department of Chemistry, University of Oxford, Physical and Theoretical Chemistry Laboratory, Oxford, United Kingdom OX1 3QZ;* orcid.org/0000-0002-8195-1232

Edward I. Brewer − *Department of Chemistry, University of Oxford, Physical and Theoretical Chemistry Laboratory, Oxford, United Kingdom OX1 3QZ*

Alice E. Green − *Department of Chemistry, University of Oxford, Physical and Theoretical Chemistry Laboratory, Oxford, United Kingdom OX1 3QZ*
Matthew Doll − *Department of Chemistry, University of Oxford, Physical and Theoretical Chemistry Laboratory, Oxford, United Kingdom OX1 3QZ*
Olga A. Duda − *Department of Chemistry, University of Oxford, Physical and Theoretical Chemistry Laboratory, Oxford, United Kingdom OX1 3QZ*

Complete contact information is available at: https://pubs.acs.org/10.1021/acs.jpca.2c07228

Author Contributions

All authors were responsible for recording data, data analysis, and interpretation of the computational work. The manuscript was written through contributions of all authors. All authors have given approval to the final version of the manuscript.

Funding

This work was funded by EPSRC Programme Grant EP/T021675 held jointly between the University of Oxford and Heriot Watt University.

Notes

The authors declare no competing financial interest.

■ ACKNOWLEDGMENTS

G.M., P.A.J.P., and E.I.B. are grateful to Worcester College, University College, and Somerville College, Oxford, respectively for financial support.

■ REFERENCES

(1) Mannucci, P. M.; Harari, S.; Martinelli, I.; Franchini, M. Effects on health of air pollution: a narrative review. *Internal and Emergency Medicine* **2015**, *10* (6), 657−662.
(2) Boningari, T.; Smirniotis, P. G. Impact of nitrogen oxides on the environment and human health: Mn-based materials for the NOx abatement. *Curr. Opin. Chem. Engin.* **2016**, *13*, 133−141.
(3) *Nitrogen oxides (NOx): why and how they are controlled*; Office of Air Quality Planning and Standards, U.S. Environmental Protection Agency: Research Triangle Park, NC, 1999.
(4) Lenner, M. Nitrogen dioxide in exhaust emissions from motor vehicles. *Atmos. Environ.* **1987**, *21* (1), 37−43.
(5) Shelef, M. Nitric Oxide: Surface Reactions and Removal from Auto Exhaust. *Catalysis Reviews* **1975**, *11* (1), 1−40.
(6) Kašpar, J.; Fornasiero, P.; Hickey, N. Automotive catalytic converters: current status and some perspectives. *Catal. Today* **2003**, *77* (4), 419−449.
(7) Koshland, D. E. The Molecule of the Year. *Science* **1992**, *258* (5090), 1861−1861.
(8) Richter-Addo, G. B.; Legzdins, P.; Burstyn, J. Introduction: Nitric Oxide Chemistry. *Chem. Rev.* **2002**, *102* (4), 857−860.
(9) Böhme, D. K.; Schwarz, H. Gas-Phase Catalysis by Atomic and Cluster Metal Ions: The Ultimate Single-Site Catalysts. *Angew. Chem., Int. Ed.* **2005**, *44* (16), 2336−2354.
(10) Blagojevic, V.; Flaim, E.; Jarvis, M. J. Y.; Koyanagi, G. K.; Bohme, D. K. Nitric Oxide as an Electron Donor, an Atom Donor, an Atom Acceptor, and a Ligand in Reactions with Atomic Transition-Metal and Main-Group Cations in the Gas Phase. *J. Phys. Chem. A* **2005**, *109* (49), 11224−11235.
(11) Klaassen, J. J.; Jacobson, D. B. Dissociative versus molecular chemisorption of nitric oxide on small bare cationic cobalt clusters in the gas phase. *J. Am. Chem. Soc.* **1988**, *110* (3), 974−976.
(12) Hanmura, T.; Ichihashi, M.; Okawa, R.; Kondow, T. Size-dependent reactivity of cobalt cluster ions with nitrogen monoxide: Competition between chemisorption and decomposition of NO. *Int. J. Mass Spectrom.* **2009**, *280* (1), 184−189.
(13) Hanmura, T.; Ichihashi, M.; Watanabe, Y.; Isomura, N.; Kondow, T. Reactions of nitrogen monoxide on cobalt cluster ions: Reaction enhancement by introduction of hydrogen. *J. Phys. Chem. A* **2007**, *111* (3), 422−428.
(14) Koyama, K.; Kudoh, S.; Miyajima, K.; Mafuné, F. Thermal Desorption Spectroscopy Study of the Adsorption and Reduction of NO by Cobalt Cluster Ions under Thermal Equilibrium Conditions at 300 K. *J. Phys. Chem. A* **2015**, *119* (37), 9573−9580.
(15) Anderson, M. L.; Ford, M. S.; Derrick, P. J.; Drewello, T.; Woodruff, D. P.; Mackenzie, S. R. Nitric oxide decomposition on small rhodium clusters, $Rh_n^{\pm}$. *J. Phys. Chem. A* **2006**, *110* (38), 10992−11000.
(16) Ford, M. S.; Anderson, M. L.; Barrow, M. P.; Woodruff, D. P.; Drewello, T.; Derrick, P. J.; Mackenzie, S. R. Reactions of nitric oxide on Rh_6^+ clusters: abundant chemistry and evidence of structural isomers. *Phys. Chem. Chem. Phys.* **2005**, *7* (5), 975−980.
(17) Harding, D.; Mackenzie, S. R.; Walsh, T. R. Structural isomers and reactivity for Rh_6 and Rh_6^+. *J. Phys. Chem. B* **2006**, *110* (37), 18272−18277.
(18) Bakker, J. M.; Mafuné, F. Zooming in on the initial steps of catalytic NO reduction using metal clusters. *Phys. Chem. Chem. Phys.* **2022**, *24* (13), 7595−7610.
(19) Yamaguchi, M.; Zhang, Y.; Lushchikova, O. V.; Bakker, J. M.; Mafuné, F. NO Bond Cleavage on Gas-Phase Ir_n^+ Clusters Investigated by Infrared Multiple Photon Dissociation Spectroscopy. *J. Phys. Chem. A* **2022**, *126* (38), 6668−6677.
(20) Fielicke, A.; von Helden, G.; Meijer, G.; Simard, B.; Rayner, D. M. Direct observation of size dependent activation of NO on gold clusters. *Phys. Chem. Chem. Phys.* **2005**, *7* (23), 3906−3909.
(21) Hayton, T. W.; Legzdins, P.; Sharp, W. B. Coordination and Organometallic Chemistry of Metal−NO Complexes. *Chem. Rev.* **2002**, *102* (4), 935−992.
(22) Blanchet, C.; Duarte, H. A.; Salahub, D. R. Density functional study of mononitrosyls of first-row transition-metal atoms. *J. Chem. Phys.* **1997**, *106* (21), 8778−8787.
(23) Thomas; Bauschlicher, C. W.; Hall, M. B. Binding of Nitric Oxide to First-Transition-Row Metal Cations: An ab Initio Study. *J. Phys. Chem. A* **1997**, *101* (45), 8530−8539.
(24) Wang, L.; Wang, G.; Qu, H.; Wang, C.; Zhou, M. Infrared Photodissociation Spectroscopy of Iron Nitrosyl Cation Complexes: $Fe(NO)_n^+$ (n = 1−5). *J. Phys. Chem. A* **2014**, *118* (10), 1841−1849.
(25) Wang, L.; Wang, G.; Qu, H.; Li, Z. H.; Zhou, M. Flexible bonding between copper and nitric oxide: infrared photodissociation spectroscopy of copper nitrosyl cation complexes: $[Cu(NO)_n]^+$ (n = 1−5). *Phys. Chem. Chem. Phys.* **2014**, *16* (22), 10788−10798.
(26) Li, Y.; Wang, L.; Qu, H.; Wang, G.; Zhou, M. Infrared photodissociation spectroscopy of mass-selected silver and gold nitrosyl cation complexes. *J. Phys. Chem. A* **2015**, *119* (15), 3577−86.
(27) Iskra, A.; Gentleman, A. S.; Kartouzian, A.; Kent, M. J.; Sharp, A. P.; Mackenzie, S. R. Infrared Spectroscopy of Gas-Phase $M^+(CO_2)_n$ (M = Co, Rh, Ir) Ion−Molecule Complexes. *J. Phys. Chem. A* **2017**, *121* (1), 133−140.
(28) Brewer, E. I.; Green, A. E.; Gentleman, A. S.; Beardsmore, P. W.; Pearcy, P.; Meizyte, G.; Pickering, J.; Mackenzie, S. R. An infrared study of CO_2 activation by holmium ions, Ho^+ and HoO^+. *Phys. Chem. Chem. Phys.* **2022**, *24*, 22716.
(29) Green, A. E.; Brown, R. H.; Meizyte, G.; Mackenzie, S. R. Spectroscopy and Infrared Photofragmentation Dynamics of Mixed Ligand Ion−Molecule Complexes: $Au(CO)_x(N_2O)_y^+$. *J. Phys. Chem. A* **2021**, *125* (33), 7266−7277.
(30) Walther, C.; Becker, S.; Dietrich, G.; Kluge, H. J.; Lindinger, M.; Lützenkirchen, K.; Schweikhard, L.; Ziegler, J. Photo fragmentation of metal clusters stored in a penning trap. *Zeitschrift für Physik D Atoms, Molecules and Clusters* **1996**, *38* (1), 51−58.
(31) Frisch, M. J.; Trucks, G. W.; Schlegel, H. B.; Scuseria, G. E.; Robb, M. A.; Cheeseman, J. R.; Scalmani, G.; Barone, V.; Petersson, G. A.; Nakatsuji, H.et al.. *Gaussian 16 Revision C.01*; Gaussian, Inc.: Wallingford, CT, 2016.

(32) Addicoat, M. A.; Metha, G. F. Kick: constraining a stochastic search procedure with molecular fragments. *J. Comput. Chem.* **2009**, *30*, 57−64.
(33) Gräfenstein, J.; Cremer, D. Can density functional theory describe multi-reference systems? Investigation of carbenes and organic biradicals. *Phys. Chem. Chem. Phys.* **2000**, *2* (10), 2091−2103.
(34) Perdew, J. P. Density-functional approximation for the correlation energy of the inhomogeneous electron gas. *Phys. Rev. B* **1986**, *33* (12), 8822−8824.
(35) Becke, A. D. Density-functional thermochemistry. III. The role of exact exchange. *J. Chem. Phys.* **1993**, *98* (7), 5648−5652.
(36) Weigend, F. Accurate Coulomb-fitting basis sets for H to Rn. *Phys. Chem. Chem. Phys.* **2006**, *8*, 1057−65.
(37) Weigend, F.; Ahlrichs, R. Balanced basis sets of split valence, triple zeta valence and quadruple zeta valence quality for H to Rn: Design and assessment of accuracy. *Phys. Chem. Chem. Phys.* **2005**, *7* (18), 3297−3305.
(38) Cunningham, E. M.; Gentleman, A. S.; Beardsmore, P. W.; Iskra, A.; Mackenzie, S. R. Infrared Signature of Structural Isomers of Gas-Phase $M^+(N_2O)_n$ (M = Cu, Ag, Au) Ion−Molecule Complexes. *J. Phys. Chem. A* **2017**, *121* (40), 7565−7571.
(39) Cunningham, E. M.; Gentleman, A. S.; Beardsmore, P. W.; Mackenzie, S. R. Structural isomers and low-lying electronic states of gas-phase $M^+(N_2O)_n$ (M = Co, Rh, Ir) ion−molecule complexes. *Phys. Chem. Chem. Phys.* **2019**, *21* (26), 13959−13967.
(40) Herzberg, G.*Molecular Spectra and Molecular Structure: II Infrared and Raman Spectra of Polyatomic Molecules*; Krieger: Malabar, FL, 1991.
(41) Dinerman, C. E.; Ewing, G. E. Infrared spectrum, structure, and heat of formation of gaseous $(NO)_2$ I. *J. Chem. Phys.* **1970**, *53* (2), 626−631.
(42) McCleverty, J. A. Chemistry of Nitric Oxide Relevant to Biology. *Chem. Rev.* **2004**, *104* (2), 403−418.

https://doi.org/10.1021/acs.jpca.2c07228
J. Phys. Chem. A 2022, 126, 9414−9422